*Tellus (2000), 52A, 75–92*


**TELLUS**
*ISSN 0280–6495*

# Implementing convection into Lorenz's global cycle.

## Part II. A new estimate of the conversion rate into kinetic energy

By LEOPOLD HAIMBERGER* and MICHAEL HANTEL, *Institut für Meteorologie und Geophysik der Universität Wien, Hohe Warte 38, A-1190 Vienna, Austria*

(Manuscript received 9 November 1998; in final form 29 April 1999)

ABSTRACT

The global conversion rates into available potential and kinetic energy (Lorenz's quantities $G$ and $C$) have been traditionally evaluated on the gridscale ($G^{\text{grid}}$, $C^{\text{grid}} \approx +2.5 \pm 0.4$ W/m$^2$). Convective phenomena acting on the sub-gridscale (like, e.g., thunderstorms) have been treated as molecular. In Part I of this study it has been outlined how Lorenz's energy cycle may be extended to include sub-gridscale processes. For this purpose new fluxes, particularly the global mean conversion rate into kinetic energy on the sub-gridscale ($C^{\text{sub}}$), have been defined. Evaluating them is the purpose of the present Part II. $C^{\text{sub}}$ is closely related to the buoyancy production term of turbulence kinetic energy which can be expressed through the vertical sub-gridscale fluxes of moisture and heat. A thermodynamic diagnostic model (DIAMOD) that estimates these fluxes indirectly from gridscale analyses is applied. In this way the conversion rate has been calculated for three months using global reanalysis data from ECMWF and from NCEP/NCAR. The errors of our results are caused by the analysis data used, by the specification of the ratio between moisture and heat fluxes (the main closure assumption in DIAMOD) and by uncertainties in the radiative heating field; they are given here at the 95% level. We find $C^{\text{sub}} = +2.2 \pm 1.7$ W/m$^2$. The new complete conversion rate $C = C^{\text{grid}} + C^{\text{sub}}$ is $+4.7 \pm 2.0$ W/m$^2$. This figure is the main result of this study, presented here for the first time: Lorenz's energy cycle, if extended to the sub-gridscale, is about twice as intense as in the traditional approximations. In contrast to $C^{\text{sub}}$ the sub-gridscale generation rate $G^{\text{sub}}$ and therefore the complete $G$ cannot be evaluated. All one can do is to improve the estimate of $G^{\text{grid}}$ by improving the estimates of the net heating. For $G^{\text{grid}}$ we find the new value of $+3.1 \pm 0.5$ W/m$^2$.

## 1. Introduction

It is a fascinating question how the general circulation of the global atmosphere is maintained against the dissipative effects of friction. Lorenz (1960) has defined the intensity of the general circulation as the global mean conversion rate $C$ from available potential energy $A$ into kinetic energy $K$. The reservoir $A$ is constantly fed by the generation rate $G$; it exchanges with the $K$ reservoir through $C$. $K$ is eventually tapped by the dissipation rate $D$. This concept leads, in the climatological mean, to

$$G = C = D. \tag{1.1}$$

This allows to estimate $C$ by estimating $G$ or to estimate both and then check the results against each other; $D$ cannot be estimated independently and is to be taken from the equivalence expressed by (1.1). As has been discussed in Part I (Hantel and Haimberger, 2000), $G$ and $C$ as understood by Lorenz (1955) are integrals of gridscale correlations. Consequently, all processes below the

* Corresponding author.
e-mail: leopold.haimberger@univie.ac.at

gridscale, including deep convection, have traditionally been treated as internal energy. This implied that the energy transfer from gridscale to sub-gridscale kinetic energy was considered as molecular dissipation.

The aim of Part I has been to drop these restrictions and come up with a generalized theory of the global energy cycle. Our approach, different from others, extends the classical energy reservoirs and conversion rates such that sub-gridscale processes are included. The ultimate reason is that the separation between gridscale and sub-gridscale is, in a sense, artificial, and has historically been dictated not by physical arguments but by the practical data availability. For the sub-gridscale quantities we use relations that can be evaluated from gridscale data by using an indirect method. We have introduced the following partitioning:

$$C = C^{\mathrm{grid}} + C^{\mathrm{sub}}, \tag{1.2}$$

where the right-hand side is defined as:

$$C^{\mathrm{grid}} = -\{\bar{\bar{\alpha}}\bar{\bar{\omega}}\}, \qquad C^{\mathrm{sub}} = -\{\overline{\overline{\alpha''\omega''}}\}. \tag{1.3}$$

The averaging operators have been defined in Section 3 of Part I. A corresponding partitioning has been introduced for $G$, $D$, $K$ and $A$. With this terminology eq. (1.1) reads in its traditional approximation:

$$G^{\mathrm{grid}} \approx C^{\mathrm{grid}} \approx D^{\mathrm{grid}}. \tag{1.4}$$

In order to proceed towards a full account of Lorenz's original equivalence one would wish to estimate also the sub-gridscale conversion terms. Due to significant progress in data accuracy and completeness over the last twenty years this task can now be tackled. The authors have put some efforts into developing an indirect method (referred to as "diagnostic model" DIAMOD) for estimating energy fluxes related to sub-gridscale processes (Hantel et al., 1993). It has so far been used for regional-scale diagnostic studies of convective systems (Haimberger et al., 1995; Hantel and Hamelbeck, 1988), recently it has been applied also for global evaluations (Hantel and Haimberger, 1998).

In Section 2, we shall show how the sub-gridscale energy fluxes diagnosed by DIAMOD can be related to sub-gridscale quantities that have been defined in Part I. In particular, the integrand $-\overline{\overline{\alpha''\omega''}}$ of the sub-gridscale conversion rate $C^{\mathrm{sub}}$ is in good approximation equal to the buoyancy flux as familiarly used in planetary boundary layer (PBL) theory (Kraus and Businger, 1994). Section 3 contains details of the numerical evaluations performed and of the input data used. The main results are presented in Section 4.

## 2. Indirectly estimating the sub-gridscale conversion terms

Some of the sub-gridscale quantities derived in Part I can be expressed in terms of sub-gridscale moisture and heat fluxes. In the following we demonstrate how these fluxes can be diagnosed indirectly from gridscale analysis data.

### *2.1. Diagnosing the buoyancy flux with DIAMOD*

The basis for the diagnostic method used (DIAMOD; see Hantel et al. (1993)) is the equation for the enthalpy of moist air $c_{\mathrm{p}}\vartheta$, with $\vartheta = T + c_{\mathrm{p}}^{-1}Lq$ referred to as equivalent temperature. In local form it reads (Ninomiya, 1968; Ninomiya, 1975):

$$\frac{\mathrm{d}c_{\mathrm{p}}\vartheta}{\mathrm{d}t} = Q_{\vartheta} + \alpha\omega. \tag{2.1}$$

The heating is defined as:

$$Q_{\vartheta} = Q_{\mathrm{rad}} - \alpha\frac{\partial}{\partial x_j}J_j^{\mathrm{q}} - \alpha\frac{\partial}{\partial x_j}J_j^{\mathrm{h}} + \varepsilon.$$

$Q_{\mathrm{rad}}$ is radiative heating, $J_j^{\mathrm{q}}$ is the latent heat flux due to molecular diffusion of water vapour, $J_j^{\mathrm{h}}$ is the molecular sensible heat flux, $\varepsilon$ is molecular dissipation. The heating $Q_{\vartheta}$ is in contrast to the net heating $Q$ of the enthalpy equation (eq. (2.3) of Part I) for dry air which contains net condensation but does not include $J_j^{\mathrm{q}}$.

The moist enthalpy equation (2.1) may be written in mass-averaged form, using standard cartesian tensor notation, as follows (compare Section 3 of Part I):

$$c_{\mathrm{p}}\left(\frac{\overline{\overline{\mathrm{d}\vartheta}}}{\mathrm{d}t} + \bar{\bar{\alpha}}\frac{\partial}{\partial x_j}\frac{1}{\bar{\bar{\alpha}}}\overline{\overline{\vartheta''v_j''}}\right) = \bar{\bar{Q}}_{\vartheta} + \bar{\bar{\alpha}}\bar{\bar{\omega}} + \overline{\overline{\alpha''\omega''}}. \tag{2.3}$$

Before we can use (2.3) for evaluating $-\overline{\overline{\alpha''\omega''}}$ some simplifications are necessary which are outlined in the following. Most atmospheric data are given in pressure coordinates. The corresponding regional mass-averaging for a quantity $k$ is defined as:

$$\overline{k} = \frac{1}{\Delta p\,\Delta A\,\Delta t}\int_{\Delta t}\int_{\Delta A}\int_{\Delta p} \times k(t, x, y, p)\,\mathrm{d}p\,\mathrm{d}A\,\mathrm{d}t, \qquad k = \overline{k} + k'. \tag{2.4}$$

This operator differs from { } defined in eq. (3.13) of Part I by the different limits; it has also been used in previous studies with DIAMOD (Haimberger et al., 1995). Here $\Delta p$ is the difference between two adjacent pressure levels, $\Delta A$ is the horizontal area of the gridcell, $\Delta t = 6$–$12$ h. Assuming that the hydrostatic equation holds on the gridscale we adopt the following approximation:

$$\overline{\overline{k}} \approx \overline{k}. \tag{2.5}$$

It allows to consider the averaged quantities diagnosed with DIAMOD as mass-averages in the sense of Part I.

As is done by most researchers (see Cotton and Anthes, 1989), the horizontal sub-gridscale and molecular flux components $\overline{\overline{\vartheta'' v_1''}}$, $\overline{\overline{\vartheta'' v_2''}}$, $J_1^{\mathrm{q}}$, $J_2^{\mathrm{q}}$, $J_1^{\mathrm{h}}$, $J_2^{\mathrm{h}}$ are all neglected while the vertical sub-gridscale component is kept and in this study is approximated as:

$$-c_{\mathrm{p}}\left[\frac{1}{\overline{\overline{\alpha}}}\overline{\overline{\vartheta'' v_3''}}\right] \approx \frac{1}{g}c_{\mathrm{p}}\overline{\vartheta'\omega'} \equiv c. \tag{2.6}$$

$c$ is the sub-gridscale enthalpy flux of moist air, introduced earlier as "total convective heat flux" (Hantel et al., 1993); here it will be referred to as convective flux.

The molecular vertical flux components $J_3^{\mathrm{q}}$ and $J_3^{\mathrm{h}}$ are active only in the less than 1 cm thick skin layer immediately above the Earth's surface (Fig. 1). It may be useful in cases to lump them into the correlation flux to yield the effective turbulent heat flux (Stull, 1988). However, we shall not adopt this convention but rather maintain that the molecular fluxes are physically different from $c$ and thus are to be kept within $Q_\vartheta$. This implies that the boundary condition for $c$ (namely, the measured latent and sensible heat fluxes, referred to as LH and SH) does not apply at the material surface of the Earth but at the top of the skin layer; this property of the $c(p)$-profile will be used below for an estimate of the net heating profile. The local dissipation rate $\varepsilon$ is typically smaller than the errors in the specification of radiative heating $Q_{\mathrm{rad}}$. We thus imply that $Q_{\mathrm{rad}}$ contains not only radiative heating but also $\varepsilon$ without specifying $\varepsilon$ explicitly. In summary, we assume that $Q_\vartheta \approx Q_{\mathrm{rad}}$ everywhere outside the skin layer.

Applying all these approximations (plus expanding $\overline{\mathrm{d}}/\mathrm{d}t$ in pressure coordinates in flux form) the moist enthalpy equation (2.3) reads with the approximations (2.5), (2.6):

$$\underbrace{c_{\mathrm{p}}\frac{\partial\bar{\vartheta}}{\partial t} + c_{\mathrm{p}}\nabla_2\cdot\bar{\vartheta}\bar{V}_2 + c_{\mathrm{p}}\frac{\partial\bar{\vartheta}\bar{\omega}}{\partial p} - \bar{\alpha}\bar{\omega} - \bar{Q}_{\mathrm{rad}}}_{\text{bud}} + \underbrace{c_{\mathrm{p}}\frac{\partial\overline{\vartheta'\omega'}}{\partial p} - \overline{\alpha'\omega'}}_{\text{sig}} = 0. \tag{2.7}$$

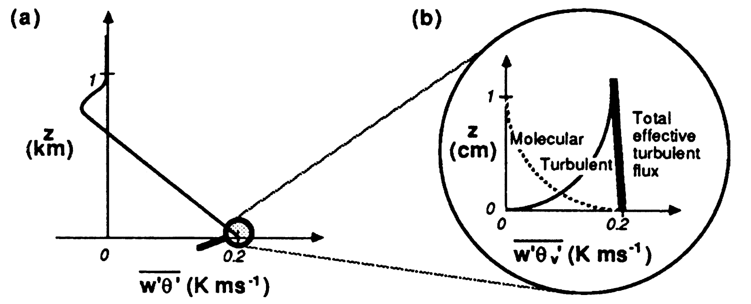


(a) The effective turbulent heat flux using daytime convective conditions as an example, may be nonzero at the surface. (b) This effective flux, however, is the sum of the actual turbulent flux and the molecular flux.

*Fig. 1.* Vertical molecular and turbulent heat flux in surface skin layer (reproduced from Stull (1988). Turbulent flux vanishes at surface due to kinematic boundary condition while molecular flux is extreme at surface and vanishes at top of skin layer.

$V_2$ is the horizontal windvector. (2.7) is identical to the convection equation (CE) of our former studies (Hantel et al., 1993; Haimberger et al., 1995; Hantel and Haimberger, 1998).

Instead of solving eq. (2.7) for the gridscale tendency $\partial\bar{\vartheta}/\partial t$ as done in forecast models (prognostic mode, *sig* parameterized) we solve the CE for the sub-gridscale quantity *sig* (diagnostic mode, $\partial\bar{\vartheta}/\partial t$ from observations). In the diagnostic mode, *bud* is considered observed and *sig* is considered unknown.

The first term in *sig* (i.e., the divergence of the convective flux) is the dominating one while the second (i.e., the buoyancy flux) is about one order of magnitude smaller. However, convective flux and buoyancy flux are coupled. This has been known from PBL theory for long (Stull, 1988; Garratt, 1992) and shall be reproduced briefly in the following.

The buoyancy flux reads:

$$-\overline{\alpha'\omega'} \approx -c_p \frac{\kappa}{p} \overline{T_v'\omega'}. \tag{2.8}$$

Here we have eliminated $\alpha$ with the virtual temperature $T_v$ and have neglected pressure fluctuations. The virtual temperature flux can be written, neglecting both triple correlations and the term $0.61\bar{q}\overline{T'\omega'}$:

$$-c_p \frac{\kappa}{p} \overline{T_v'\omega'} = = -c_p \frac{\kappa}{p} \overline{\{(\bar{T}+T')(1+0.61[\bar{q}+q'])\}\omega'} \approx -c_p \frac{\kappa}{p} [\overline{T'\omega'} + 0.61\bar{T}\overline{q'\omega'}]. \tag{2.9}$$

We further introduce the relation between temperature flux and moisture flux in form of the inverse Bowen ratio in the atmosphere (Hantel, 1987):

$$\frac{L\overline{q'\omega'}}{c_p\overline{T'\omega'}} \equiv \frac{1}{\beta}. \tag{2.10}$$

The inverse Bowen ratio $1/\beta(p)$ is an unknown function of pressure to be specified externally (see below); this is equivalent to a closure assumption. With it the temperature and the moisture flux take on the forms:

$$\frac{c_p}{g}\overline{T'\omega'} = \frac{1}{1+1/\beta}c, \qquad \frac{L}{g}\overline{q'\omega'} = \frac{1/\beta}{1+1/\beta}c. \tag{2.11}$$

Upon combining eqs. (2.8)–(2.11) we obtain:

$$-\overline{\alpha'\omega'} \approx -\frac{g}{p} \underbrace{\kappa \frac{1+(0.61c_p\bar{T}/L)1/\beta}{1+1/\beta}}_{\tilde{\kappa}} c. \tag{2.12}$$

Considering $\bar{T}(p)$ and $1/\beta(p)$ as gridscale functions of pressure, eq. (2.12) allows to calculate the profile $-\overline{\alpha'\omega'}(p)$ of the buoyancy flux once the profile $c(p)$ of the convective flux has been estimated. The gridscale function $\tilde{\kappa}(p)$ is for dry conditions (moisture flux zero) identical to $\kappa = R/c_p$. For moist conditions $\tilde{\kappa}(p)$ deviates from $\kappa$; the deviation is controlled by the inverse Bowen ratio profile.

Due to the coupling between buoyancy flux and convective flux eq. (2.7) can be written as ordinary differential equation in pressure:

$$\mathrm{bud}(p) + g\frac{\mathrm{d}c(p)}{\mathrm{d}p} - g\frac{\tilde{\kappa}(p)}{p}c(p) = 0. \tag{2.13}$$

The CE in the form (2.13) can be solved by standard methods. The boundary condition at the surface is $c(p_s) = \mathrm{LH} + \mathrm{SH}$; the surface fluxes LH, SH are considered turbulent above the skin layer.

The CE is the key for diagnosing the sub-gridscale processes of our extended energy cycle. Once the solution $c(p)$ has been found, the buoyancy flux can be computed in every gridbox of an atmospheric column and, upon global integration, yields the sub-gridscale conversion rate $C^{\mathrm{sub}}$.

### 2.2. *Diagnosing the heating rate with DIAMOD*

One of the achievements that came with Lorenz's energy cycle is that estimates of $C$ can be checked with independent estimates of $G = \{NQ\}$. The main problem in calculating $G$ is to estimate the net heating rate $Q$ defined in eq. (2.1) of Part I (which is different from $Q_\vartheta$). The following processes, sorted after their magnitude on the global scale, contribute to $Q$: radiative heating, latent heat release, heating due to molecular heat conduction and dissipation. The most straightforward option, equivalent to how we have treated $Q_\vartheta$ above, would be to approximate $Q$ by radiation plus latent heating. However, specification of latent heating from observations is too inaccurate. Thus, following various authors (Hantel and Baader, 1978; Hoskins et al., 1989; Fortelius, 1995), we evaluated the heating rate $Q$ indirectly by employing the dry enthalpy equation:

$$Q = \underbrace{\frac{\mathrm{d}c_p T}{\mathrm{d}t} - \alpha\omega}_{R}. \tag{2.14}$$

$R$ can be interpreted as the response of the atmosphere to diabatic forcing. Expanding $R$ and averaging yields with approximations consistent with the ones used in deriving eq. (2.7):

$$\bar{R} = \underbrace{c_p \frac{\partial \bar{T}}{\partial t} + c_p \nabla_2 \cdot \bar{T}\bar{V}_2 + c_p \frac{\partial \bar{T}\bar{\omega}}{\partial p} - \bar{\alpha}\bar{\omega}}_{\bar{R}^{\mathrm{grid}}} + \underbrace{c_p \frac{\partial \overline{T'\omega'}}{\partial p} - \overline{\alpha'\omega'}}_{\bar{R}^{\mathrm{sub}}}. \tag{2.15}$$

The idea is that $\bar{R}$ has to be equal to the forcing $\bar{Q}$. The sub-gridscale response $\bar{R}^{\mathrm{sub}}$ should be included since it does not need to be small (Hantel and Baader, 1978).

The generation rate $G = \{NR\}$ can now be separated into:

$$G^{\mathrm{grid}} = \underbrace{\{\bar{N}\bar{R}^{\mathrm{grid}}\}}_{G_*^{\mathrm{grid}}} + \{\bar{N}\bar{R}^{\mathrm{sub}}\}, \quad G^{\mathrm{sub}} = \{\overline{N'R'}\}. \tag{2.16}$$

In previous estimates of the generation rate (Siegmund, 1994) only $G_*^{\mathrm{grid}}$ has been evaluated. The contribution $\bar{N}\bar{R}^{\mathrm{sub}}$ has been neglected since the sub-gridscale quantities in $\bar{R}^{\mathrm{sub}}$ have been considered molecular.

With the formulae (2.11) and (2.12) both components of $\bar{R}^{\mathrm{sub}}$ can now be expressed in terms of the convective flux. Thus we can calculate the complete $G^{\mathrm{grid}}$. $G^{\mathrm{sub}}$ is still not evaluable at present.

However, when trying to evaluate $\bar{R}^{\mathrm{sub}}$, and opposite to the situation when evaluating the buoyancy flux, we encounter a new problem. It is caused by the skin layer immediately above the Earth's surface (thickness less than 1 cm, mass $\Delta p$ less than $10^{-6}$ of the mass of the total atmosphere) in which $\bar{Q}$, represented by $\bar{R}^{\mathrm{sub}}$ in (2.15), reaches extreme values. The reason is the huge divergence of $\overline{T'\omega'}$ in the skin layer. In contrast, the formula (2.12) for $-\overline{\alpha'\omega'}$ does not require differentiation.

In order to estimate the term $\{\bar{N}\bar{R}^{\mathrm{sub}}\}$ we split the averaging over the mass of the atmosphere into two parts, one over the atmosphere above the skin layer and one over the skin layer:

$$\frac{1}{M}\int_M \bar{N}\bar{R}^{\mathrm{sub}}\,\mathrm{d}M = \frac{1}{p_s A}\int_A \int_0^{p_s - \Delta p} \bar{N}\bar{R}^{\mathrm{sub}}\,\mathrm{d}p\,\mathrm{d}A + \frac{1}{p_s A}\int_{\mathrm{A}} \int_{p_s - \Delta p}^{p_s} \bar{N}\bar{R}^{\mathrm{sub}}\,\mathrm{d}p\,\mathrm{d}A. \tag{2.17}$$

Above the skin layer, $\bar{R}^{\mathrm{sub}}$ has moderate values and can be diagnosed with DIAMOD. Thus we can readily evaluate the first integral on the rhs. of (2.17).

The second integral cannot be evaluated with DIAMOD. This is reflected in the lower boundary value of $\overline{T'\omega'}$ in DIAMOD, which is equal to $gc_p^{-1}SH$, valid at the top of the skin layer. Exactly at the Earth's surface $\overline{T'\omega'}$ is zero since there can be no turbulent transport through a material surface. Thus there is rapid divergence of $\overline{T'\omega'}$ within the skin layer. This property of the turbulent flux $\overline{T'\omega'}$ is illustrated in Fig. 1 from the textbook of Stull (1988). It is important to recognise that $\overline{T'\omega'}$ in the present context is not the effective flux (= the sum of molecular and turbulent flux) since it does not contain the molecular flux $J_3^{\mathrm{h}}$. The molecular forcing $\bar{Q}$ is dominated by the convergence of the molecular heat flux and the response $\bar{R}$ is almost exclusively represented by the extreme divergence of $\overline{T'\omega'}$; both effects balance each other in the skin layer.

From these arguments the second integral of (2.17) can be approximated as follows:

$$\frac{1}{p_s A}\int_A \int_{p_s - \Delta p}^{p_s} \bar{N}\bar{R}^{\mathrm{sub}}\,\mathrm{d}p\,\mathrm{d}A \approx \frac{c_p}{p_s A}\int_A \int_{p_s - \Delta p}^{p_s} \bar{N}\frac{\mathrm{d}\overline{T'\omega'}}{\mathrm{d}p}\,\mathrm{d}p\,\mathrm{d}A \approx -\frac{g}{p_s A}\int_A \bar{N} SH\,\mathrm{d}A. \tag{2.18}$$

Here we have neglected the second term of $\bar{R}^{\mathrm{sub}}$ in (2.15) and have assumed that the efficiency factor in the skin layer is constant in the vertical; thus $\bar{N}\bar{R}^{\mathrm{sub}}$ becomes independent upon the poorly known thickness $\Delta p$.

We conservatively adopt for $\bar{N}$ the value near the Earth's surface where it is almost everywhere positive (Dutton and Johnson, 1967; note, however, that this neglects the Θ-dependence of $p_r$ and thus of $\bar{N}$ within the skin layer). Further, since $SH$ is reasonably well known, at least the sign and the order of magnitude of $\bar{N}\bar{R}^{\text{sub}}$ can be estimated with the approximation (2.18). We expect that $\bar{N}$ is positively correlated with $-SH$ which yields a systematic and nonnegligible contribution to $G^{\text{grid}}$.

We are now ready to evaluate $C^{\text{grid}}$, $C^{\text{sub}}$ and the improved $G^{\text{grid}}$ from general circulation data.

## 3. Input data and numerical issues

Preliminary estimates of $C^{\text{sub}}$ have been gained with operational initialized analyses of the European Centre for Medium-Range Weather Forecasts (ECMWF) for August 1991 (Haimberger and Hantel, 1996; Haimberger, 1998); a value of 2.8 W/m$^2$ has been found, but it has been concluded that the data input must be improved to get a reliable estimate of $C^{\text{sub}}$.

In the present paper we use primarily reanalysed data for the gridscale atmospheric budget terms. These have been generated in delayed mode by the European Re-Analysis (ERA) project performed at ECMWF (Gibson et al., 1996) and by the National Center for Environmental Prediction (NCEP)/National Center for Atmospheric Research (NCAR) reanalysis project, respectively (Kalnay et al., 1996). The highest available resolution has been taken for each data source (T106L31 model level data for ERA, T62L28 model level data for NCEP, 6 hourly intervals).

All terms of bud in eq. (2.7) except $Q_{\text{rad}}$ have been calculated from these input data using the original discretization schemes of the assimilating models (pressure hybrid coordinates, semi-Lagrangian advection in the ECMWF-model, Eulerian advection in the NCEP/NCAR forecast model) in order to avoid interpolation errors. These are not always small and can blur the physical signal as has been discussed by Haimberger et al. (1995); Trenberth (1995); Calanca and Fortelius (1996). The gridscale bud has been evaluated with DIAMOD in $120 \times 60$ atmospheric columns of equal area covering the whole globe.

To solve the CE (2.13), further input is needed. The field of $Q_{\text{rad}}$ has been taken from ERA (6–18 hourly forecasts) and NCEP/NCAR (0–6 hourly forecasts since longer term forecasts have not been available) as a substitute for satellite observations which are not available in the needed vertical resolution. For the specification of the lower boundary condition of the CE we used the corresponding forecast latent and sensible heat fluxes LH and SH, respectively, as a substitute for observations.

It has been noted by the providers of the reanalysed data sets that the products gained from forecasts should be used with caution. Thus we have performed some consistency tests with the forecast radiation and surface energy flux fields.

As is well known, the surface fluxes LH, SH should balance the net radiative flux difference between bottom and top of the atmosphere in the global mean*. If this is not the case, the atmosphere would cool down or heat up. This behaviour should also be found in global forecast models and can be used to detect systematic forecast errors (Klinker and Sardeshmukh, 1992). As a matter of fact, $\{Q_{\text{rad}}\}$ and $\{LH\} + \{SH\}$ do not balance in the first hours of the forecasts of the assimilating models. The imbalance in the first 6 h of the forecasts is 20 W/m$^2$ in the ERA model and 13 W/m$^2$ in the NCEP/NCAR model for January 1993. Consequently, the model atmospheres of both ERA and NCEP/NCAR model show a spurious cooling trend of up to 0.4 K/day in the global mean in some atmospheric layers (Fig. 2). It is caused by a systematic error either in $\{Q_{\text{rad}}\}$ or $\{\text{LH}\} + \{\text{SH}\}$ or in both.

This misfit cannot be tolerated. Since the cooling trend disappears after about 2–3 forecast days it would seem an option to avoid it by using fluxes from longer term forecasts as input data; however, it is undesirable to use forecasts longer than 12–18 h since the model atmospheres may have drifted towards a possibly unrealistic "model climate".

The second option is to remove the misfit in the short-term forecast flux fields. We performed two different modifications of these forecast input fields.

- In the first modification we assume that $LH + SH$ is correct and the misfit is caused by the

* The other terms on the rhs. of the globally averaged moist enthalpy equation (2.3), $-\{\alpha\omega\}$ and $\{\varepsilon\}$, are much smaller and should also balance.

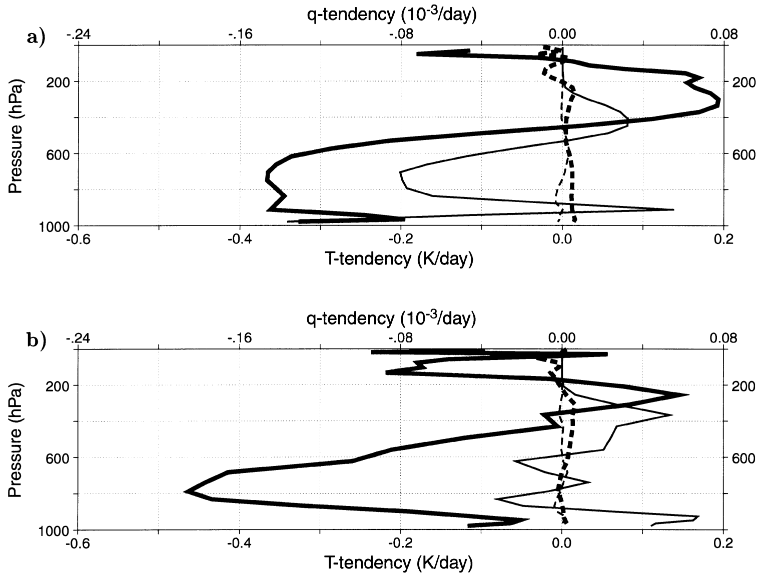


*Fig. 2.* Global mean forecast (solid) and analysed (dashed) tendencies of heat (thick curves, bottom $x$-axis, units K/day) and moisture (thin curves, top $x$-axis, units $10^{-3}$/day), averaged over January 1993. (a) From 6-hourly ERA-forecasts/analyses, (b) from 6-hourly NCEP/NCAR-forecasts/analyses. Differences between forecast and analysed tendencies are systematic tendency errors.

radiative heating field (too strong radiative cooling). The model bias may be measured as the monthly mean difference between analysed tendency and forecast tendency as shown in Fig. 2. Thus we add the difference between forecast equivalent temperature tendency and analysed equivalent temperature tendency to the $Q_{\mathrm{rad}}$ field. This reduces the misfit between $Q_{\mathrm{rad}}$ and $LH+SH$ by an order of magnitude. To remove the imbalance completely would be possible but not useful since for monthly means, as discussed here, small deviations from radiative-convective equilibrium can occur. The modified $Q_{\mathrm{rad}}$ is then consistent in the global mean with $LH+SH$ and the analysed equivalent temperature tendency. Fig. 3 shows the vertical profile of the resulting modification of $Q_{\mathrm{rad}}$ in the global monthly mean.

• In the other modification we assume that $Q_{\mathrm{rad}}$ is correct. In this case we add the vertically integrated systematic equivalent temperature tendency forecast error to $LH+SH$ in every atmospheric column. This leads to stronger surface fluxes in almost all latitudes (see Fig. 4). The global mean $1/\beta$ ($\approx 5$) at the surface remains nearly unchanged by this modification.

Both modifications have their merits. The modification of $Q_{\mathrm{rad}}$ corrects the misfit in every atmospheric layer. This is particularly important since the tendency errors tend to be positive in high and negative in low layers. Thus they introduce a spurious slope into the bud-profile (see Haimberger et al., 1995) that is corrected with the $Q_{\mathrm{rad}}$-modification. On the other hand the modification of $LH+SH$ is weaker due to the partial compensation of the tendency errors in the vertical. Further it is known that $LH+SH$ tends to be too weak in the first hours of the forecasts (Kållberg, 1998). The best guess is probably a combination of modifications.

The global data inconsistencies as demonstrated in Figs. 2–4 are principally relevant and contribute significantly to the errors encountered in the final results of this study. However, as we shall see later, the modification mode chosen does not have much impact upon value and accuracy of $C^{\mathrm{sub}}$.

The second principal error source is due to our ignorance concerning the profile of the inverse Bowen ratio $1/\beta$ which must be specified for the CE (2.13) to be solved. Since $L\overline{q'\omega'}$ and $c_{\mathrm{p}}\overline{T'\omega'}$ are driven by the same eddy velocity it seems

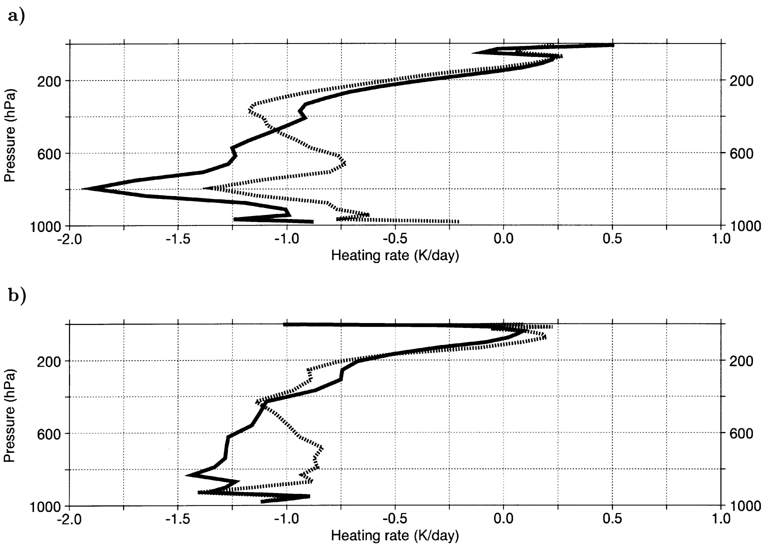


*Fig. 3.* Global horizontal monthly mean of unmodified (solid) and modified (dashed) $Q_{\mathrm{rad}}$, (a) from twice daily ERA-forecasts (forecast hours 6–18), (b) from four times daily NCEP/NCAR-forecasts (forecast hours 0–6). Values in units K/day, valid for January 1993.

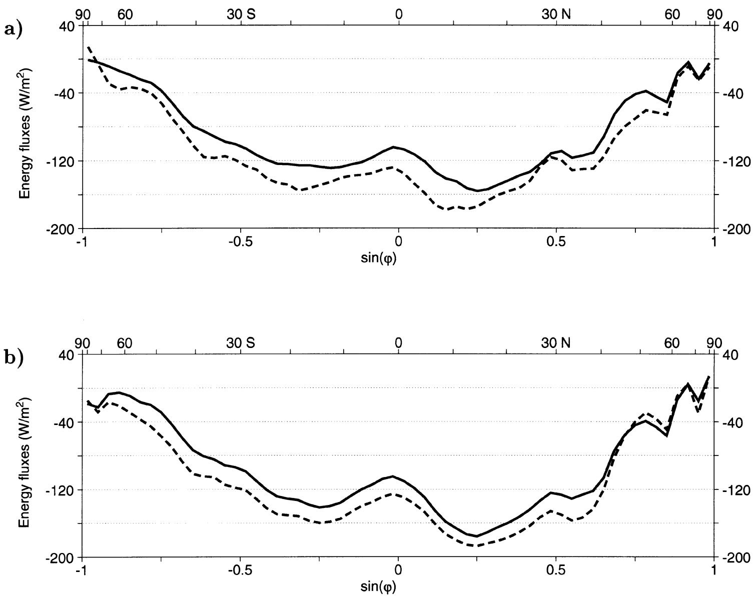


*Fig. 4.* Zonal monthly mean of unmodified (solid) and modified (dashed) $LH + SH$, (a) from twice daily ERA-forecasts (forecast hours 6–18), (b) from four times daily NCEP/NCAR-forecasts (forecast hours 0–6). Values in units W/m$^2$, valid for January 1993.

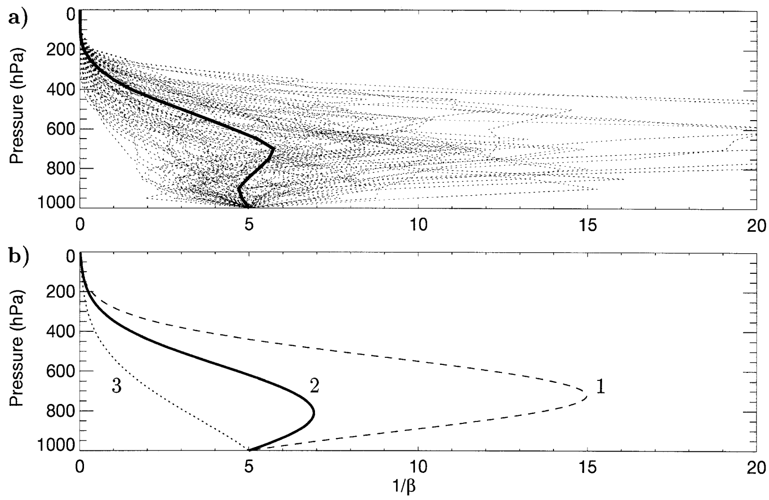


*Fig. 5.* (a) Ratio of gridscale variance of $c_p T$ and $Lq$ within 72 regions regularly distributed over the Earth. Size of regions: $(3000\ \mathrm{km})^2$; size of gridscale columns: $(300\ \mathrm{km})^2$. Thin curves: profiles of ratio in each region. Thick curve: global average of profiles. (b) Idealized profiles of $1/\beta$. Thick solid profile 2 designed to closely match mean profile in (a). The other two profiles 1, 3 are used in sensitivity experiments.

plausible that $L\overline{q'\omega'}$ may be proportional to the sub-gridscale moisture variance and $c_p\overline{T'\omega'}$ proportional to the sub-gridscale horizontal temperature variance. The various $1/\beta$ profiles in Fig. 5a have been calculated from gridscale variances on areas of $(3000\ \mathrm{km})^2$ all over the globe. The thick curve is the mean over all those ratios of variances. This profile shall be used as the standard profile in the following evaluations. It is scaled with the ratio $1/\beta(p_s) = LH/SH$ at the surface in the individual columns. A similar result is independently obtained if we approximate $1/\beta$ by the ratio of the global mean gridscale moisture flux and heat flux (not shown).

In addition to the thick $1/\beta$ profile in Fig. 5a two other profiles are chosen that account for the inherent uncertainty in the specification of the global mean $1/\beta$ profile visible in Fig. 5a. The results of a couple of sensitivity experiments performed with the three $1/\beta$ profiles shown in Fig. 5b are discussed below.

## 4. Results

Here we document results from evaluations of gridscale and sub-gridscale energy conversion rates for three months, January 1993, July 1996 and January 1997 from the data sets noted above.

We first show our evaluations of the classical conversion terms. Fig. 6 displays vertical zonal monthly means of the integrands of $G_*^{\mathrm{grid}}$ and $C^{\mathrm{grid}}$. The integrand $\bar{N}\bar{R}^{\mathrm{grid}}$ shows maximum values near the ITCZ, where the atmosphere is heated at relatively high temperatures and at high latitudes where it is cooled at low temperatures.

The integrand $-\bar{\alpha}\bar{\omega}$ of $C^{\mathrm{grid}}$ shows a broad positive maximum in the tropics and broad negative maxima in the subtropics, reflecting the Hadley cell; thus $-\bar{\alpha}\bar{\omega}$ is subject to considerable compensation, the mean value is only about 1% of the standard deviation. Alternatively one can also evaluate $-\bar{V}_2 \cdot \nabla_2 \bar{\Phi}$ since for gridscale data the implied hydrostatic assumption is totally acceptable (Peixóto and Oort, 1974). In this case the compensation is much less and the global mean value is thus less prone to numerical errors. The values for $C^{\mathrm{grid}}$ presented here are therefore global means of $-\bar{V}_2 \cdot \nabla_2 \bar{\Phi}$.

Our best estimates for the global averages over the three months investigated are $G_*^{\mathrm{grid}} = 2.6 \pm 0.4\ \mathrm{W/m^2}$ and $C^{\mathrm{grid}} = 2.5 \pm 0.4\ \mathrm{W/m^2}$. The error values are twice the standard deviations of the mean values. Though not strictly comparable due to the short time averaging interval they are quite in accord with results in the literature (Arpe et al., 1986; Peixóto and Oort, 1992; Siegmund,

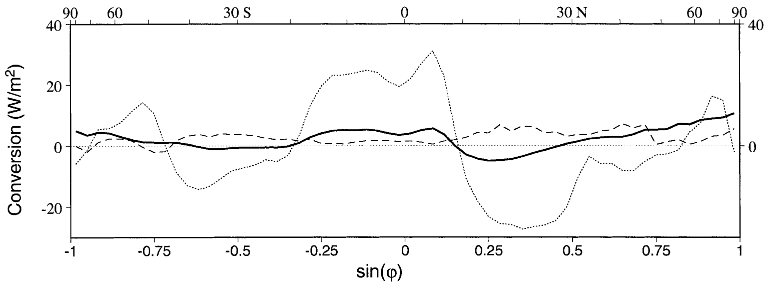


*Fig. 6.* Zonal monthly mean of vertically integrated $\bar{N}\bar{R}^{\mathrm{grid}}$ (solid), of vertically integrated $-\bar{\alpha}\bar{\omega}$ (dotted, multiplied with 0.1) and of vertically integrated $-\bar{V}_2 \cdot \nabla_2 \bar{\Phi}$ (dashed). Curves valid for January 1993, calculated from ERA data. Corresponding global means are 2.3 W/m$^2$, 2.4 W/m$^2$ and 2.6 W/m$^2$, respectively.

1994). The remaining part of $G^{\mathrm{grid}}$ (which is subgridscale) will be discussed further below.

We now move to the evaluation of $C^{\mathrm{sub}}$. Fig. 7 shows zonal mean plots of $c(p)$. Panel (a), generated with ERA-data, exhibits the typical distribution of $c(p)$: Maximum negative values near the surface in the subtropics of the northern hemisphere, corresponding to a permanent upward convective flux beginning at the Earth's surface and converging in upward direction to about tropopause level. A second maximum of $c(p)$ can be found in the tropical mid-troposphere. Slightly positive (i.e., downward directed) values of $c(p)$ prevail at and above the tropopause and in polar regions.

A qualitatively similar picture can be found when using NCEP/NCAR reanalysis data (Fig. 7b). However there are sizeable differences in the tropics and subtropics between panels (a) and (b). No maximum of $c(p)$ in the tropical mid-troposphere can be found in the evaluations of the NCEP/NCAR reanalyses and the subtropical surface fluxes are larger. Since the global observation data source for the two reanalyses was similar for both centres the differences of the $c(p)$ fluxes must mainly stem from differences in the representation of various physical processes in the assimilating models (Hantel and Haimberger, 1998). However this cannot be avoided when using analysis data. We have also evaluated $c(p)$ with corrected $LH+SH$; the differences between the $c(p)$ fluxes from ERA and NCEP/NCAR are about the same (not shown).

Figs. 8, 9 show the zonal monthly mean of the buoyancy flux $-\overline{\alpha'\omega'}$. The differences between the four panels due to data and evaluation method uncertainties are not small. However, the main features are invariant: The typical order of magnitude in the zonal mean is $10^{-3}$ W/kg. Further, $-\overline{\alpha'\omega'}$ is positive throughout the troposphere with maximum values in the PBL and in the tropical upper troposphere. Only in the stratosphere and near the poles negative values prevail, consistent with the small positive $c(p)$-values in the stratosphere noted in Fig. 7.

So far only the sensitivity to the modification of $Q_{\mathrm{rad}}$ and of $LH+SH$ and the sensitivity with respect to the analysis data sources has been tested; the $1/\beta$ profile has been kept fixed. The next step is to vary the $1/\beta$ profiles. While the impact of $1/\beta(p)$ on $c(p)$ is very small (not shown but extensively discussed in Hantel et al. 1993; Haimberger et al., 1995) this is different for the buoyancy flux. Fig. 10 shows the monthly mean of $-\overline{\alpha'\omega'}$ in a meridional section, Fig. 11 in a vertical section. The integrand is the larger the smaller $1/\beta$. The three $1/\beta$ profiles have a visible impact upon the size of the integrand, but not upon its sign. The integrand with maximum values of more than 5 W/m$^2$ in the tropics is positive almost everywhere except in the polar regions; therefore the global mean $C^{\mathrm{sub}}$ is also positive and typically within the range $2.2 \pm 1.0$ W/m$^2$. A similar result is found when using NCEP/NCAR data (Table 1). The vertical profiles of the horizontally averaged $-\overline{\alpha'\omega'}$ (Fig. 11) are positive except above the troposphere where comparatively small negative values can be found. The impact of $1/\beta$ on $-\overline{\alpha'\omega'}$ is strongest in the mid-troposphere. In summary, the error due to $1/\beta$ is comparable to the error sources of the assimilating models.

The values of $C^{\mathrm{sub}}$ obtained are summarized in Table 1, including results for July 1996 and January 1997. The three-month survey indicates

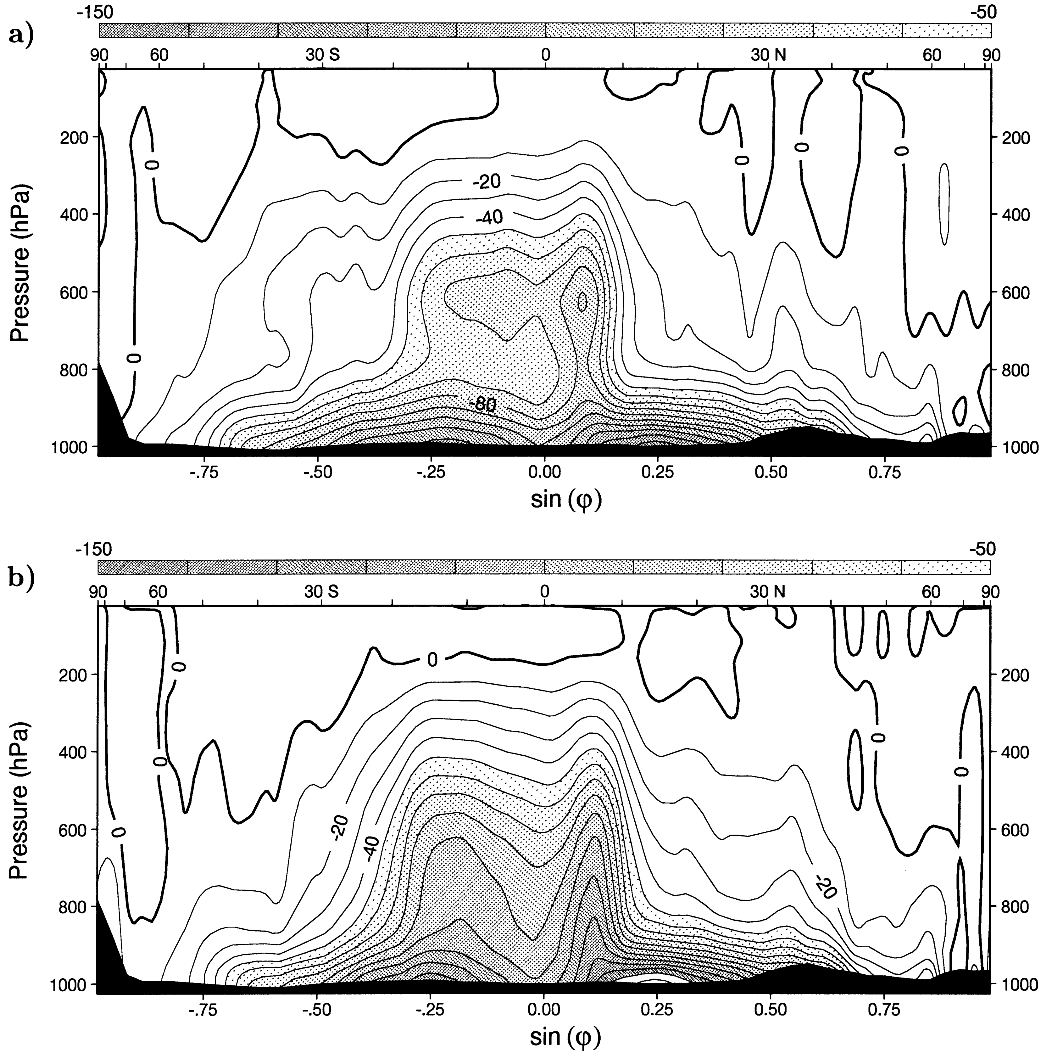


*Fig. 7.* Zonal monthly mean of $c(p)$ with corrected $Q_{\mathrm{rad}}$. Values in units W/m$^2$ valid for January 1993. $c(p)$ calculated with thick $1/\beta$ profile of Fig. 5b. Black regions at bottom indicate zonal mean orography. Upper abscissa geographical latitude $\phi$, lower abscissa sin $\phi$. (a) Pattern calculated from ERA data; (b) from NCEP/NCAR data.

that $C^{\mathrm{sub}}$ is larger if $Q_{\mathrm{rad}}$ is corrected instead of $LH + SH$, particularly when ECMWF data are used. $C^{\mathrm{sub}}$ is consistently larger (about 1 W/m$^2$ on average) with NCEP/NCAR than with ERA reanalyses, particularly when $LH + SH$ is corrected.

From the results above we conclude that sign and order of magnitude of $C^{\mathrm{sub}}$ can be estimated fairly reliably although the error of $C^{\mathrm{sub}}$ is sizeable. The 95% confidence interval for $C^{\mathrm{sub}}$ calculated from the 36 values of Table 1, assuming normal distribution, is:

$$C^{\mathrm{sub}} = 2.2 \pm 1.7 \ \mathrm{W/m^2}. \tag{4.1}$$

Our next evaluation concerns the components of $G^{\mathrm{grid}}$. The zonally, vertically and monthly averaged integrands $\bar{N}\bar{R}^{\mathrm{grid}}$ and $\bar{N}\bar{R}^{\mathrm{sub}}$ are shown in Fig. 12. The globally mass-averaged $\bar{N}\bar{R}^{\mathrm{sub}}$ in the atmosphere above the skin layer is slightly negative ($-0.0$ to $-0.4$ W/m$^2$) while it is positive

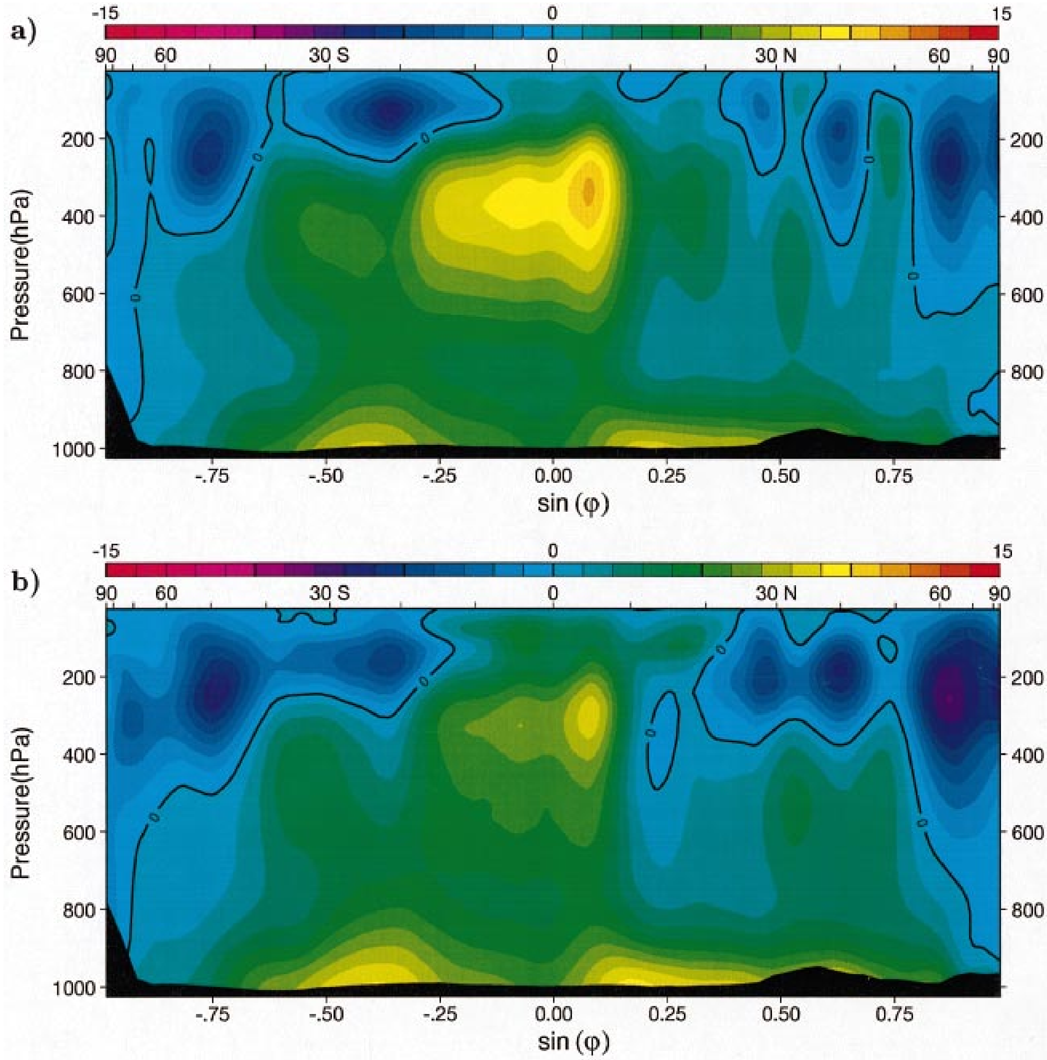


*Fig. 8.* Zonal monthly mean of buoyancy flux $-\overline{\alpha'\omega'}$ calculated from ERA data with thick $1/\beta$ profile of Fig. 5b. Panel (a) with corrected $Q_{\mathrm{rad}}$, (b) with corrected $LH+SH$. Black regions at bottom indicate zonal mean orography. Values in units $10^{-4}$ W/kg valid for January 1993.

($\approx 0.6$ W/m$^2$) in the skin layer, resulting in values of $\{\bar{N}\bar{R}^{\mathrm{sub}}\}$ between 0.2 and 0.6 W/m$^2$ (see also Table 2, limited to ECMWF data).

This strong influence of the skin layer is consistent with the fact that the destabilizing effect due to the convergence of the molecular flux $J_3^{\mathrm{h}}$ is concentrated in the skin layer. $J_3^{\mathrm{h}}$ generates unstable vertical temperature stratifications that eventually lead to non-molecular motion above the skin layer; in other words, it feeds an energy reservoir available for conversion into kinetic energy.

The range of values in Fig. 12 is the result of a sensitivity experiment in which the $1/\beta$ profile has been varied according to Fig. 5b. The error of $\bar{N}\bar{R}^{\mathrm{sub}}$ due to uncertainties in specifying $1/\beta$ is not too large. Yet, one should not forget that a constant $\bar{N}$ in the skin layer (extrapolated from calculated values in the boundary layer above) has been used in order to evaluate this term. Further, we

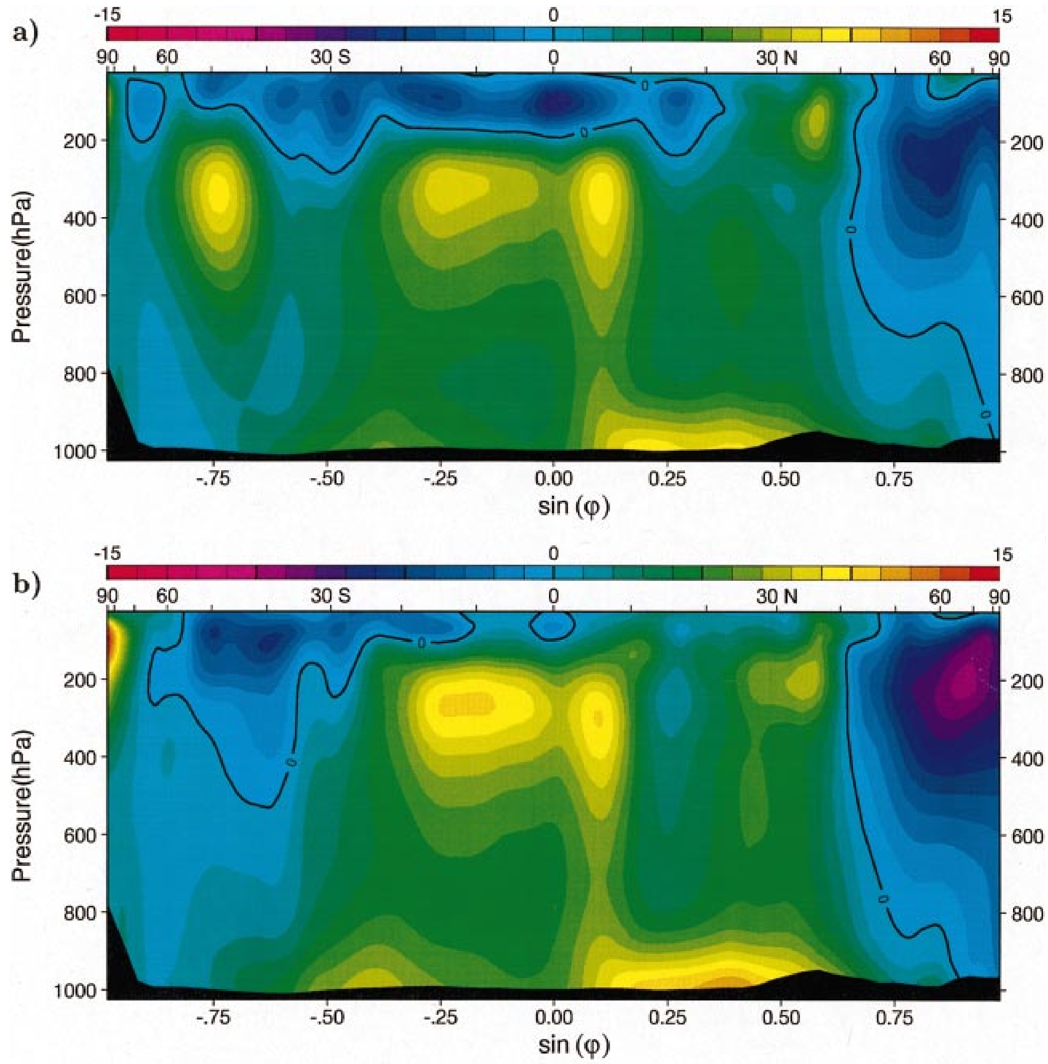


*Fig. 9.* As Fig. 8 but calculated from NCEP/NCAR instead of ERA data.

needed $Q_{\mathrm{rad}}$ as input to get first bud, then $c(p)$ and finally $\bar{N}\bar{R}^{\mathrm{sub}}$. This implies that we had to specify a part of $\bar{Q}$ (namely, $Q_{\mathrm{rad}}$ and the divergence of $J_3^{\mathrm{h}}$ in the skin layer) in order to get the complete $\bar{R}$ (= $\bar{Q}$ including latent heat release). Despite these uncertainties sign and order of magnitude of $\{\bar{N}\bar{R}^{\mathrm{sub}}\}$ are physically plausible.

Our results are graphically summarized in Fig. 13 which is similar to that in Lorenz (1967). It shows the global conversion rates between the gridscale plus sub-gridscale reservoirs of available potential energy ($A$) and of kinetic energy ($K$). Figures without brackets have been calculated from general circulation data. This applies in the first place to the components of $C$. Because of eq. (1.1) knowing the complete $C$ is sufficient to specify the intensity of the generalized Lorenz energy cycle. The figures with brackets correspond to quantities that cannot be evaluated directly since their integrands are unavailable. An example is $G^{\mathrm{sub}}$ whose integrand $\overline{N'R'}$ cannot be evaluated. We have estimated $G^{\mathrm{sub}}$ as residual by assuming that the reservoirs $A$ and $K$ are constant in time.

We have further assumed, in accord with the

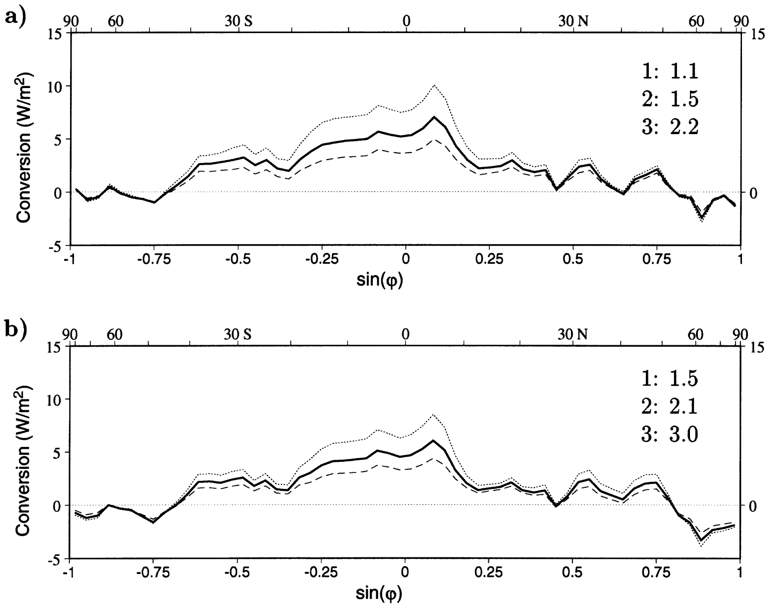


*Fig. 10.* Zonal-vertical integrals of $-\overline{\alpha'\omega'}$, time-averaged over January 1993, in units W/m$^2$, from ERA-data. Three curves in each panel generated with $1/\beta$ profiles of Fig. 5b. (a) Calculated with corrected $Q_{\mathrm{rad}}$. (b) Calculated with corrected $LH + SH$.

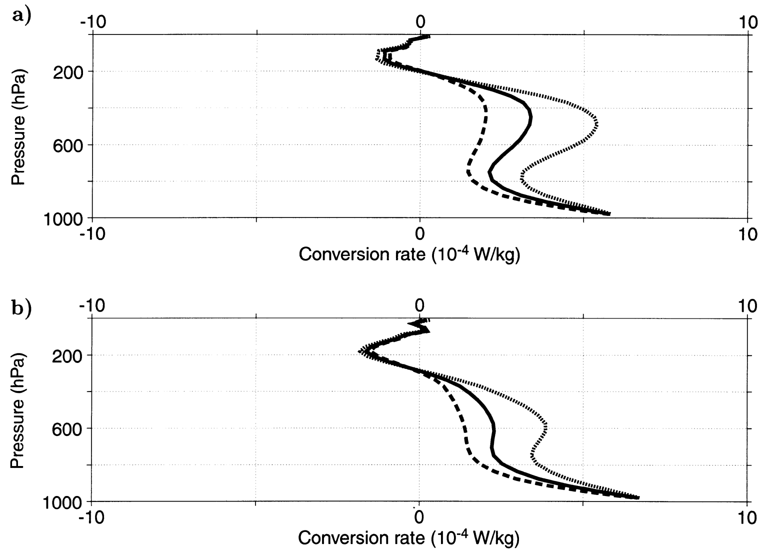


*Fig. 11.* Global horizontal averages of $-\overline{\alpha'\omega'}$-profiles, time-averaged over January 1993, in units $10^{-4}$ W/kg, from ERA-data. Three curves in each panel generated with $1/\beta$ profiles of Fig. 5b. (a) Calculated with corrected $Q_{\mathrm{rad}}$. (b) Calculated with corrected $LH + SH$.

Table 1. *Mean values of $C^{sub}$ for 3 different months, calculated from ECMWF data (reanalysis data for January 1993, operational analysis data for July 1996 and January 1997) and NCEP/NCAR reanalysis data using different corrections and $1/\beta$ profiles (see text); values are in units W/m²*

| Data source | $Q_{rad}$ corrected | | | $LH+SH$ corrected | | |
|---|---|---|---|---|---|---|
| $1/\beta$ profile | 1 | 2 | 3 | 1 | 2 | 3 |
| 9301,ERA | 1.5 | 2.1 | 3.0 | 1.1 | 1.5 | 2.2 |
| 9301,NCEP | 1.8 | 2.4 | 3.0 | 1.8 | 2.4 | 3.2 |
| 9607,ECMWF | 1.5 | 2.1 | 3.0 | 0.8 | 1.2 | 1.9 |
| 9607,NCEP | 2.4 | 3.2 | 4.1 | 2.3 | 3.1 | 4.1 |
| 9701,ECMWF | 1.2 | 1.8 | 2.6 | 0.5 | 0.8 | 1.3 |
| 9701,NCEP | 2.4 | 3.0 | 3.8 | 1.8 | 2.4 | 3.2 |

Table 2. *Monthly mean values of $\bar{N}\bar{R}^{sub}$ for 3 different months, calculated from ECMWF data using different corrections and $1/\beta$ profiles (see text); values are in units W/m²*

| Data source | $Q_{rad}$ corrected | | | $LH+SH$ corrected | | |
|---|---|---|---|---|---|---|
| $1/\beta$ profile | 1 | 2 | 3 | 1 | 2 | 3 |
| 9301,ERA | 0.2 | 0.4 | 0.6 | 0.2 | 0.3 | 0.4 |
| 9607,ECMWF | 0.4 | 0.4 | 0.5 | 0.4 | 0.5 | 0.5 |
| 9701,ECMWF | 0.2 | 0.2 | 0.2 | 0.2 | 0.2 | 0.2 |

literature, that the gridscale dissipation $D^{\text{grid}}$ is negligible. We maintain that the kinetic energy of large-scale motions is first converted into smaller scale eddies before it can be dissipated. Our results suggest that the small-scale eddies are fed at about equal amounts by shear production (which must be equal to $C^{\text{grid}}$ if $D^{\text{grid}}$ is negligible) and by buoyant production $C^{\text{sub}}$. Our best estimate for the dissipation rate $D^{\text{sub}}$ which can be considered as the total dissipation rate is 4.7 W/m², about twice as large as previous estimates.

## 5. Conclusions

The goal of this study has been to extend the classical energy cycle of Lorenz (1955), Lorenz (1967), towards including sub-gridscale processes. Up to now the sub-gridscale fluxes could not be evaluated mainly for practical reasons. Consequently, the kinetic energy of, for example, cumulus convection has been treated as internal energy.

In Part I of this study we have tried to generalize Lorenz's theory to include also sub-gridscale motions while retaining the form of the generation rate $G=\{NQ\}$, of the conversion rate $C=-\{\alpha\omega\}$ and of the dissipation rate $D$. Taking into account both components of $G=G^{\text{grid}}+G^{\text{sub}}$ and of $C=C^{\text{grid}}+C^{\text{sub}}$ brings Lorenz's concept to its full potential.

In the present Part II we have tried to evaluate gridscale and sub-gridscale contributions to $G$ and $C$ from the reanalysed data sets of the ECMWF (Gibson et al., 1996) and of NCEP/NCAR (Kalnay et al., 1996). These are presently the best data sources for evaluations of the global energy cycle. Since the data are available on pressure surfaces we have adopted the approximations:

$$\begin{aligned} &\overline{\overline{N}}\,\overline{\overline{Q}} \approx \overline{N}\,\overline{Q}, \qquad \overline{\overline{N''Q''}} \approx \overline{N'Q'}, \\ &-\overline{\overline{\alpha}}\,\overline{\overline{\omega}} \approx -\overline{\alpha}\,\overline{\omega}, \qquad -\overline{\overline{\alpha''\omega''}} \approx -\overline{\alpha'\omega'}. \end{aligned} \tag{5.1}$$

The double bars and double primes refer to the exact mass averaging operator discussed in Part I,

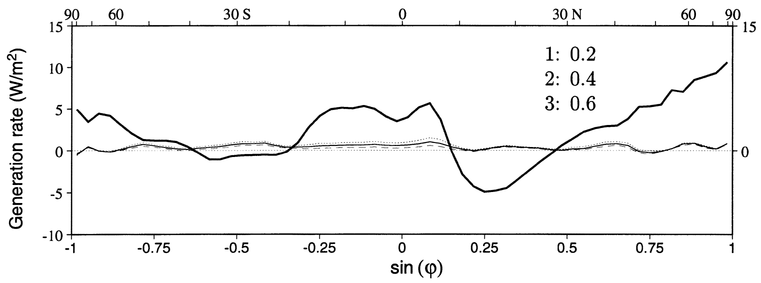


*Fig. 12.* Zonal-vertical integrals of $\bar{N}\bar{R}^{\text{grid}}$ (thick curve, mass average 2.6 W/m²) and $\bar{N}\bar{R}^{\text{sub}}$ (three curves, line style corresponding to $1/\beta$ profiles as shown in Fig. 5b), time-averaged over January 1993. All curves calculated with modified $Q_{\text{rad}}$, from ERA data. Numbers denote global mass averages of $\bar{N}\bar{R}^{\text{sub}}$ profiles (W/m²).

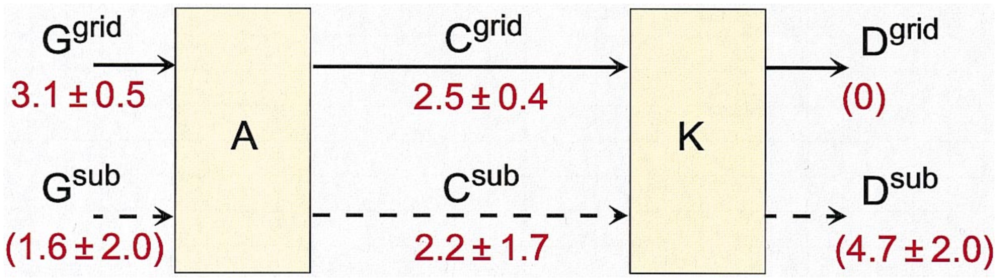


*Fig. 13.* Completed global energy cycle. $A$ = available potential energy; $K$ = kinetic energy. The conversion terms $G^{\mathrm{grid}}$, $C^{\mathrm{grid}}$, $D^{\mathrm{grid}}$ comprise the traditional quanties. The quantites $G^{\mathrm{sub}}$, $C^{\mathrm{sub}}$, $D^{\mathrm{sub}}$ are the new sub-gridscale conversion fluxes, evaluated here for the first time. Numbers without brackets in units W/m$^2$ calculated from global atmospheric data. Numbers with brackets indirectly estimated assuming that reservoirs $A$ and $K$ are stationary. Errors of numbers shown are discussed in text.

the single bars and single primes to the approximate averaging operator performed on the $p$-surfaces. Thus our evaluations have yielded:

$$G^{\mathrm{grid}} \approx \{\bar{N}\bar{Q}\}, \qquad G^{\mathrm{sub}} \approx \{\overline{N'Q'}\},$$
$$C^{\mathrm{grid}} \approx -\{\bar{\alpha}\bar{\omega}\}, \qquad C^{\mathrm{sub}} \approx -\{\overline{\alpha'\omega'}\}. \tag{5.2}$$

The braces denote the global averaging operator performed on the gridscale.

Concerning $C$ we have noted that the integrand of $C^{\mathrm{sub}} = -\{\overline{\alpha'\omega'}\}$ is identical to the familiar buoyancy flux in the turbulence kinetic energy equation. It can be expressed by the turbulent moisture and heat fluxes in the atmosphere (Stull, 1988) which are principally observable at a single location. The problem has been to evaluate these fluxes on the global scale. For this purpose we have employed a thermodynamic diagnostic model (DIAMOD, Hantel et al., 1993; Haimberger et al., 1995) which yields estimates of the turbulent heat fluxes. The gridscale analysed data from the reanalyses have been the main data source. In addition the surface flux fields $LH$, $SH$ as well as the 3D radiative heating field as forecast by the assimilating models used for the reanalyses have been employed. These modelled input data are not error-free. Further errors in the analysed data sets and in the main closure assumption used in DIAMOD introduce additional uncertainty into $C^{\mathrm{sub}}$.

Despite these limitations the buoyancy flux has been found to be positive in practically all latitudes in all our sensitivity experiments. This suggests that the results are systematic and not accidental. Best estimate for $C^{\mathrm{sub}}$ is $2.2 \pm 1.7$ W/m$^2$.

A basic problem, not solved in this study, is that we do not know to what extent our results are influenced by the sub-gridscale parameterizations of the assimilating models. This problem is typical for all conclusions to be drawn from evaluations that make use of modern reanalysis data sets. It might seem interesting in this context to evaluate $-\overline{\alpha'\omega'}$ from sub-gridscale fluxes as parameterized in GCMs. We do not consider this too useful, however, since these fluxes are typically calculated with the equation for moist static energy (Tiedtke, 1989) in which $-\overline{\alpha'\omega'}$ is neglected (Yanai and Johnson, 1993). Alternatively $-\overline{\alpha'\omega'}$ could be calculated with cloud resolving models (CRMs) which model the buoyancy flux explicitly, and to compare the corresponding CRM conversion terms with our diagnostic estimates (although such a comparison would presently be restricted to selected regions). We have postponed such experiments to future studies. In the present study we have focussed exclusively to the diagnostic aspect.

The gridscale component $C^{\mathrm{grid}} = -\{\bar{\alpha}\bar{\omega}\}$ can be calculated directly from the gridscale analysed data. The best estimate for three months evaluated is $2.5 \pm 0.4$ W/m$^2$. It follows that the complete $C = C^{\mathrm{grid}} + C^{\mathrm{sub}}$ amounts to $4.7 \pm 2.0$ W/m$^2$, more than twice the value of classical estimates (Peixóto and Oort, 1992). This figure represents our main result. It resolves also the three decades old discrepancy between Lorenz's dissipation estimate (about 2.0 W/m$^2$) and independent estimates reported by Newell et al. (1970), as discussed above in Part I (about 6.0 W/m$^2$).

Concerning $G$ we have argued that previous estimates of $G^{\mathrm{grid}} = \{\bar{N}\bar{Q}\}$ have suffered from neglecting the sub-gridscale energy flux divergences when indirect estimates of $\bar{Q}$ are employed. The indirect technique calculates the atmospheric response $\bar{R}$ that balances $\bar{Q}$ defined in (2.15). However, $\bar{R}$ is implicitly partitioned into $\bar{R}^{\mathrm{grid}}$ and $\bar{R}^{\mathrm{sub}}$. In the traditional evaluations, $G^{\mathrm{grid}}$ has been assumed to be the global mass average of $\bar{N}\bar{R}^{\mathrm{grid}}$. In our study, we have tried to evaluate also $\bar{R}^{\mathrm{sub}}$; this has been principally possible since $\bar{R}^{\mathrm{sub}}$ can be related to the sub-gridscale sensible heat flux diagnosed by DIAMOD. Correlating $\bar{R}^{\mathrm{grid}} + \bar{R}^{\mathrm{sub}}$ with $\bar{N}$ should give an improved estimate of $G^{\mathrm{grid}}$.

When trying to implement this program, major difficulties (that Lorenz has predicted in 1955) have been encountered since in the surface skin layer $\bar{R}^{\mathrm{sub}}$ reaches extreme values. We had to assume a constant $\bar{N}$ in order to evaluate the contribution to $G^{\mathrm{grid}}$ from the skin layer. This is a rather crude assumption. Our estimates yield $G^{\mathrm{grid}} = 3.1 \pm 0.5$ W/m$^2$ where $2.6 \pm 0.4$ W/m$^2$ stem from $\{\bar{N}\bar{R}^{\mathrm{grid}}\}$ and $0.4 \pm 0.2$ W/m$^2$ from $\{\bar{N}\bar{R}^{\mathrm{sub}}\}$.

We consider the central outcome of this study, namely, that the complete conversion rate $C$ into kinetic energy is about 4.7 W/m$^2$, as a novel result. It implies that Lorenz's classical estimate of $C$ lacks the contribution of the sub-gridscale. Our results suggest that the intensity of the complete global energy cycle as measured by $C$ is about twice as high as the present textbook figure.

At the end of this exercise one might argue that most of the kinetic energy generated at the sub-gridscale is also dissipated at the sub-gridscale before interaction with larger scales takes place and that our estimate of $C^{\mathrm{sub}}$, although new, does not change our view of the global energy cycle in a deeper sense.

Our data do not quite support this criticism. From Fig. 13 we see that $G^{\mathrm{sub}}$ is smaller than $C^{\mathrm{sub}}$ (if allowance is made for the high error level). This requires that there is an additional flux of potential energy from the gridscale into the sub-gridscale, in accord with theories of deep convection (Emanuel, 1994) which identify large scale ascent as a source for convective available potential energy.

This interpretation suggests that the separability of gridscale kinetic energy ("synoptic dynamics") and sub-gridscale kinetic energy ("convective dynamics") may be less ideal than implied by the traditional expositions of the global energy cycle. The dynamics of thunderstorms cannot be adequately described with the notion of molecular friction. Rather, the gridscale and sub-gridscale branches are intimately coupled. We have tried here, in a first step and with limited and noisy data, to point towards a quantitative appraisal of this global coupling.

## 6. Acknowledgements

This work has been financially supported by the Austrian Fonds zur Förderung der Wissenschaftlichen Forschung, Project P11764-GEO. We thank the European Centre for Medium-Range Weather Forecasts (Special Project "Estimating the global mean sub-gridscale conversion term into kinetic energy", 1996–1998), the National Center for Atmospheric Research as well as the Austrian Zentralanstalt für Meteorologie und Geodynamik, for providing data and computer facilities. We further appreciate useful suggestions by F. Hamelbeck. A couple of points raised by the anonymous reviewers helped to clarify our arguments.

REFERENCES

Arpe, K., Brankovic, C., Oriol, E. and Speth, P. 1986. Variability in time and space of energetics from a long series of atmospheric data produced by ECMWF. *Beitr. Phys. Atmos.* **59**, 321–355.

Calanca, P. and Fortelius, C. 1996. Representation of model data and evaluation of diagnostic equations in pressure coordinates. *Tellus* **48A**, 756–766.

Cotton, W. and Anthes, R. A. 1989. *Storm and cloud dynamics*, vol. 44 of *Int. Geophys. Ser.* Academic Press, 883 pp.

Dutton, J. A. and Johnson, D. R. 1967. The theory of available potential energy and a variational approach to atmospheric energetics. *Adv. Geophys.* **12**, 333–437.

Emanuel, K. A. 1994. *Atmospheric convection.* Oxford University Press, 580 pp.

Fortelius, C. 1995. Inferring the diabatic heat and moisture forcing of the atmosphere from assimilated data. *J. Climate* **8**, 224–239.

Garratt, J. R. 1992. *The atmospheric boundary layer.* Cambridge University Press, 316 pp.

Gibson, J. K., Kålberg, P. and Uppala, S. 1996. The ECMWF re-analysis (ERA) project. *ECMWF Newsletter* **73**, 7–17.

Haimberger, L. 1998. Estimating the conversion rate into kinetic energy of sub-gridscale motions. *Phys. Chem. Earth* **23**, 623–628.

Haimberger, L. and Hantel, M. 1996. Extension of Lorenz's energy cycle to the sub-gridscale. In: *Preprint Volume of the Second International Scientific Conference on the Global energy and water cycle*, 17–21 June 1996, Washington DC, USA, pp. 308–309. GEWEX-WCRP.

Haimberger, L., Hantel, M. and Dorninger, M. 1995. A thermodynamic diagnostic model for the atmosphere. Part III: DIAMOD with orography and new error model. *Meteorol. Z., N.F.* **4**, 162–182.

Hantel, M. 1987. Subsynoptic vertical heat fluxes from high resolution synoptic budgets. *Meteorol. Atmos. Phys.* **36**, 24–44.

Hantel, M. and Baader, H. R. 1978. Diabatic heating climatology of the zonal atmosphere. *J. Atmos. Sci.* **35**, 1180–1189.

Hantel, M., Ehrendorfer, M. and Haimberger, L. 1993. A thermodynamic diagnostic model for the atmosphere. Part II: The general theory and its consequences. *Meteorol. Z., N.F.* **2**, 255–271.

Hantel, M. and Haimberger, L. 1998. Diagnosing convection from global analyses. *Meteorol. Atmos. Phys.* **67**, 135–152.

Hantel, M. and Haimberger, L. 2000. Implementing convection into Lorenz's global cycle, Part I: Gridscale averaging of the energy equations. *Tellus* **52A**, 66–74.

Hantel, M. and Hamelbeck, F. 1998. Convective activity quantified by sub-gridscale fluxes. *Phys. Chem. Earth* **23**, 649–654.

Hoskins, B. J., Hsu, H. H., James, I. N., Masutani, M., Sardeshmukh, P. D. and White, G. H. 1989. *Diagnostics of the global atmospheric circulation.* WCRP-27. WMO, 217 pp.

Kållberg, P. 1998. Fluxes and some other surface characteristics of ERA. In: *Proceedings of the 1st International Conference on Reanalyses.* Silver Spring MD, WMO-TD-NO 876, CH-1211 Geneva 2, Switzerland, pp. 93–96. WMO.

Kalnay, E., Kanamitsu, M., Kistler, R., Collins, W., Deaven, D., Gandin, L., Iredell, M., Saha, S., White, G., Woollen, J., Zhu, Y., Chelliah, M., Ebisuzaki, W., Higgins, W., Jawoniak, J., Mo, K. C., Ropelewski, C., Wand, J., Leetmaa, A., Reynolds, R., Jenne, R. and Joseph, D. 1996. The NCEP/NCAR 40-year reanalysis project. *Bull. Amer. Meteorol. Soc.* **77**, 437–471.

Klinker, E. and Sardeshmukh, P. D. 1992. The diagnosis of mechanical dissipation in the atmosphere from large-scale budget requirements. *J. Atmos. Sci.* **49**, 608–627.

Kraus, E. B. and Businger, J. A. 1994. *Atmosphere–ocean interaction.* Oxford University Press, 362 pp.

Lorenz, E. N. 1955. Available potential energy and the maintenance of the general circulation. *Tellus* **7**, 157–167.

Lorenz, E. N. 1960. Energy and numerical weather prediction. *Tellus* **12**, 364–373.

Lorenz, E. N. 1967. *The nature and theory of the general circulation of the atmosphere*, Vol. 218.TP.115. WMO, 161 pp.

Newell, R. E., Vincent, D. G., Dopplick, T. G., Ferruzza, D. and Kidson, J. W. 1970. The energy balance of the global atmosphere. In: *The global circulation of the atmosphere* (ed. Corby, G. A.), pp. 42–90. London: Roy. Met. Soc.

Ninomiya, K. 1968. Heat and water budget over the Japan sea and the Japan islands in winter seasons – with special emphasis on the relation among the supply from the sea surface, the convective transfer and the heavy snowfall. *J. Meteor. Soc. Jap.* **46**, 343–372.

Ninomiya, K. 1975. Large-scale aspects of air-mass transformation over the East China Sea during AMTEX '74. *J. Meteor. Soc. Jap.* **53**, 285–303.

Peixóto, J. P. and Oort, A. H. 1974. The annual distribution of atmospheric energy on a planetary scale. *J. Geophys. Res.* **79**, 2149–2159.

Peixóto, J. P. and Oort, A. H. 1992. *Physics of climate.* American Institute of Physics, 520 pp.

Siegmund, P. 1994. The generation of available potential energy, according to Lorenz' exact and approximate equations. *Tellus* **46A**, 566–582.

Stull, R. B. 1988. *An introduction to boundary layer meteorology.* Kluwer Academic Publishers, 666 pp.

Tiedtke, M. 1989. A comprehensive mass flux scheme for cumulus parameterization in large-scale models. *Mon. Wea. Rev.* **117**, 1779–1800.

Trenberth, K. E. 1995. Truncation and use of model–coordinate data. *Tellus* **47A**, 287–303.

Yanai, M. and Johnson, R. H. 1993. Impacts of cumulus convection on thermodynamic fields. In: *The representation of cumulus convection in numerical models* (eds. Emanuel, K. A. and Raymond, D. J.), vol. 24 of Meteorological monographs, pp. 39–62. Boston, Massachusetts: American Meteorological Society.